CIRP Annals - Manufacturing Technology 62 (2013) 527–530

Contents lists available at SciVerse ScienceDirect

CIRP Annals - Manufacturing Technology

journal homepage: http://ees.elsevier.com/cirp/default.asp

Study on nano thickness inspection for residual layer of nanoimprint lithography using near-field optical enhancement of metal tip

S. Takahashi (2)*, Y. Ikeda, K. Takamasu

Department of Precision Engineering, The University of Tokyo, Hongo 7-3-1, Bunkyo-ku, Tokyo 113-8656, Japan

ARTICLE INFO

Keywords:
Inspection
Optical
Nanoimprint lithography

ABSTRACT

We propose a novel nano thickness inspection method of residual layer film of nanoimprint lithography, allowing nondestructive evaluation of residual layer thickness independent of the diffraction limit. In the proposed method, we applied near-field optical enhancement of a fine metal tip as a high spatial resolution measurement probe, with which we can get near-field optical response generated by dynamic interaction of the tip, thin residual layer film and a Si substrate. By performing theoretical analyses based on finite-difference time-domain (FDTD) method and fundamental experiments using a newly developed near-field optical response detection system, we verified the feasibility of the proposed method.

1. Introduction

Nanoimprint lithography (NIL), allowing fabrication of micro/nanometer scale features with low cost, high throughput and high resolution [1–3], is one of the best candidates for meeting the requirement of the next-generation semiconductor patterning [4]. The process steps of UV-based NIL (Fig. 1) are as follows: (I) A mold made of transparent material like fused silica, quartz with nano-patterns on its surface is pressed into the resin layer on the Si substrate, after dispensing a UV-curable liquid photopolymer as resist on a Si substrate. (II) The resist is cured by UV light exposure and becomes solid. (III) The mold is realized from the solidified resin. (IV) Here, a thin resin layer with thickness of several 10s nm remains as a residual film (residual layer) between the imprinted patterns and the Si substrate. (V) Finally, a reactive ion etching (RIE) is performed to remove the residual layer. (VI) As a result, we can form fine patterns on the Si substrate like conventional photolithography. In the NIL process, in order to get the fine resist mask patterns accurately, an optimization of the RIE based on the residual layer thickness (RLT) is one of the most important factors. Therefore, in order to realize the NIL as a next-generation semiconductor photolithography process with high reliability, it is urgently needed to develop a nondestructive evaluation technique of the RLT, allowing optimization the RIE condition of the NIL processes [5,6].

There are various types of nondestructive thin film thickness measurement techniques [7–10]. Especially, optical methods such as ellipsometer and white light interferometer are well known for their nondestructiveness [11,12]. It is true that these optical thickness measurement methods have superior resolution power about 1 nm scale in the vertical resolution, but have lack of the lateral resolution due to the diffraction limit. Therefore, it is difficult to directly apply the conventional optical thickness measurement methods to evaluation of the RLT of the NIL processes because the residual layer is located only between the fine structure patterns, lateral size of which is less than 100 nm. On the other hand, the cross-sectional scanning electron microscopy (SEM) meets the requirement of its fine lateral resolution, but the cross-section imaging requires the physical cleaving of the device, meaning destructive process [13]. Up to the present time there has been no useful method to evaluate RLT without using the cross-sectional SEM, while even discrimination between the 10-nm-scale-RLT and the 50-nm-scale-RLT nondestructively is useful for adjusting the RIE conditions.

In order to improve the lateral resolution of optical method beyond the diffraction limit, we have proposed an application of near-field optics [14] to inspection of the RLT of NIL. We have already developed the RLT measurement system using the near-field optical fiber probe [15,16]. It is true that measurement method based on near-field optics does not depend on the diffraction limit but the lateral resolution of the fiber-type near-field optical probe is almost 100 nm, which means that it doesn't meet the next-generation fine semiconductor patterns with the half pitch of 20 nm scale, and moreover, the amount of the near-field optical response obtained with the fiber-type near-field optical probe is too weak to evaluate its signal with high-signal-to noise ratio. In order to overcome the abovementioned problems, in this research, by taking the advantage of the diffraction limit free characteristics of the near-field optics, we propose a novel RLT inspection method of NIL using a near-field optical enhancement of a sharp metal probe instead of a fiber-type probe.

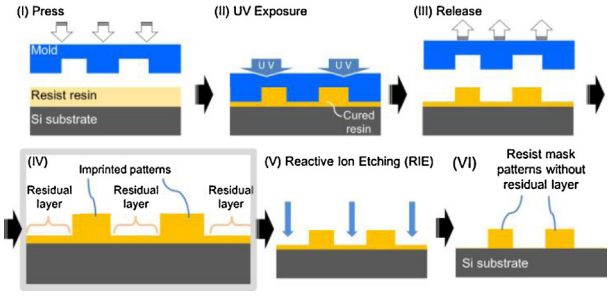

Fig. 1. Process steps of UV-cured NIL for semiconductors.

* Corresponding author.

0007-8506/$ – see front matter © 2013 CIRP.
http://dx.doi.org/10.1016/j.cirp.2013.03.020

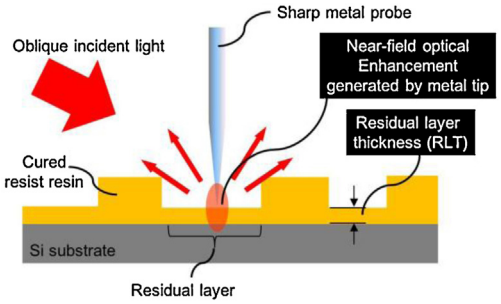

Fig. 2. Concept of proposed method using near-field optical enhancement by metal tip.

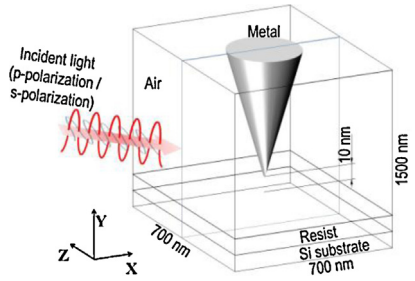

Fig. 3. Simulation model for near-field optical enhancement analyses.

2. Concept of nano thickness inspection of RLT using near-field optical enhancement of metal tip

Fig. 2 shows a schematic diagram of the new concept of the RLT inspection method for NIL using near-field optical enhancement of metal tip. In order to get the information of RLT, a sharp metal probe with the tip diameter of 10 nm scale is set just above residual layer located between fine patterns formed with NIL. Sample surface is obliquely illuminated with gently focused incident light. Under this condition, at the vicinity of the metal tip, localized light energy can be generated by near-field optical enhancement of metal tip [17,18]. This enhanced light energy, the size of which does not depend on the diffraction limit but mainly on the tip size, is so localized that this can interact with only the area of the residual layer of NIL sample. Therefore, by detecting the far-field propagating light which is radiated from the interaction of the enhanced light with the Si substrate through the residual layer film, information of RLT is expected to be analyzed.

3. Numerical simulation based on FDTD method

3.1. Simulation model

Firstly, we tried to confirm the proposed concept theoretically. Here, in order to analyze detailed behavior of near-field optical enhancement, we performed numerical simulations using a finite-difference time-domain (FDTD) method [19], with which three dimensional electric field vector components interacted with arbitral material structures can be numerically calculated.

Fig. 3 shows typical FDTD simulation model employed in this research. 5-nm-unit cells with the simulation range of

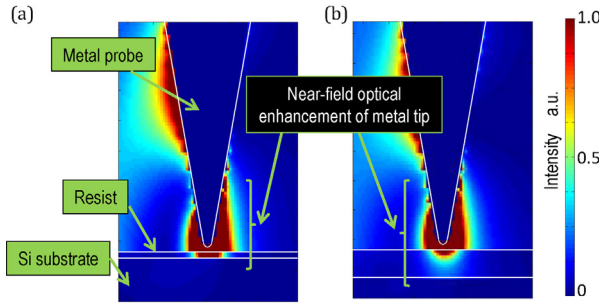

Fig. 4. Calculated intensity distribution [p-polarized incident light/*XY*-plane]. (a) RLT: 10 nm. (b) RLT: 50 nm.

700 nm × 700 nm × 1500 nm were set. As an initial study, we treated flat thin resist film as the residual layer to analyze the optical enhancement interacted with metal tip, residual layer, and Si substrate. A metal probe tip made of silver having the tip diameter of 15 nm was modeled with the gap distance of 10 nm from top surface of residual resist layer. As the external light illuminator, a plane wave with the wavelength of 632.8 nm, assuming a He–Ne laser, was employed, incident angle of which was 45°.

3.2. Near-field optical enhancement characteristics of metal tip interacted with residual layer and Si substrate

Fig. 4 shows numerically calculated intensity distributions on *XY*-plane including central axis of the metal probe with the RLT of 10 nm (a) and 50 nm (b), respectively, where p-polarized incident light is employed. We see that an optical intensity enhancement can generate at the vicinity of the metal tip and this enhancement gets into the residual resist layer.

Next, in order to carry out detailed analyses of behavior of the interacted enhancement, three dimensional electric field vector components were calculated. In Figs. 5(a), (b) and 6(a), (b) visualize electric field vector components under p-polarized incident light with the RLT of 10 nm and 50 nm, respectively. Fig. 5 means result on the *XY*-plane including central axis of the metal probe and Fig. 6 means one on the *YZ*-plane. The *Ez* component (*z*-component of electric field) of Fig. 5 and the *Ex* component of Fig. 6 cannot be observed well, but both the *Ex* and the *Ey* components of Fig. 5 and both the *Ey* and the *Ez* components of Fig. 6 surround the metal probe with higher amplitude. Taken together, the *Ex* component and the *Ez* component are also enhanced depend on the polarization of the incident light and the metal tip structure, but only the enhanced *Ey* component can get into the residual resist layer, which suggests that detecting the *Ey* component from the near-field optical enhancement of the metal tip plays an important role for analyzing the RLT. On the other hand, in the case of s-polarized incident light, distinct enhancement of the metal tip interacted with the residual resin and the Si substrate was not found under various conditions. (Fig. 7 is a typical example in the case of s-polarized incident light.)

3.3. Far-field optical response from near-field optical enhancement

Next, we estimated intensity of far-field propagating light radiated from the near-field optical enhancement, which can be detected for the RLT evaluation in the practical situation. Fig. 8

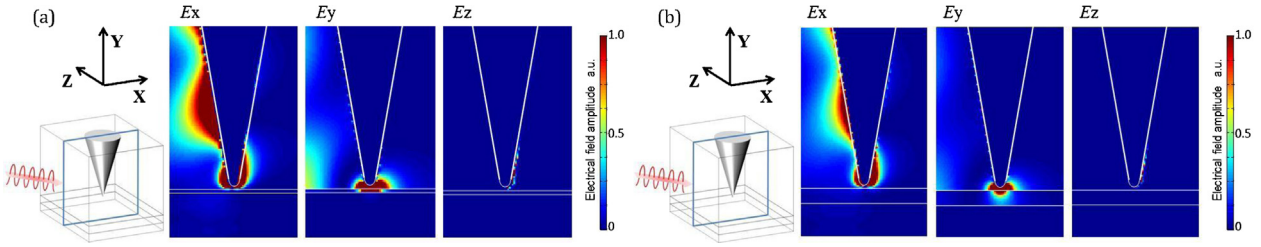

Fig. 5. Three dimensional electric field components under p-polarized incident light [*XY*-plane]. (a) RLT:10 nm. (b) RLT:50 nm.

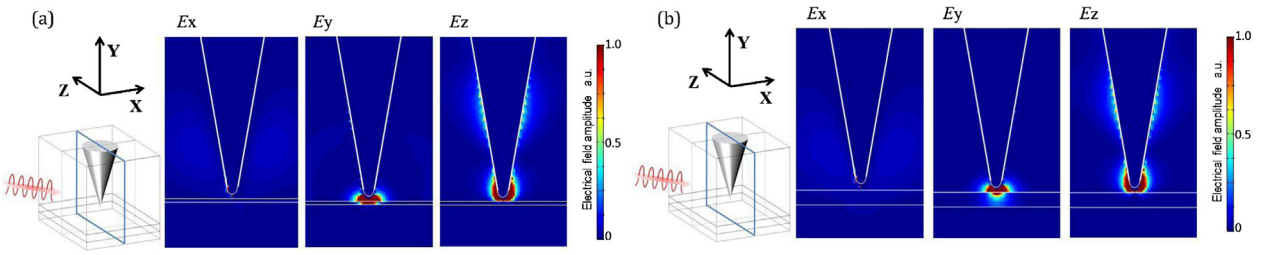

Fig. 6. Three dimensional electric field components under p-polarized incident light [*YZ*-plane]. (a) RLT: 10 nm. (b) RLT: 50 nm.

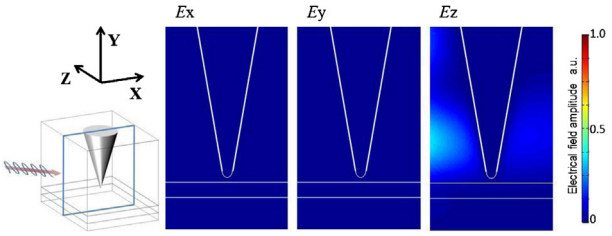

Fig. 7. Typical result under s-polarized incident light [RLT: 50 nm/*XY*-plane].

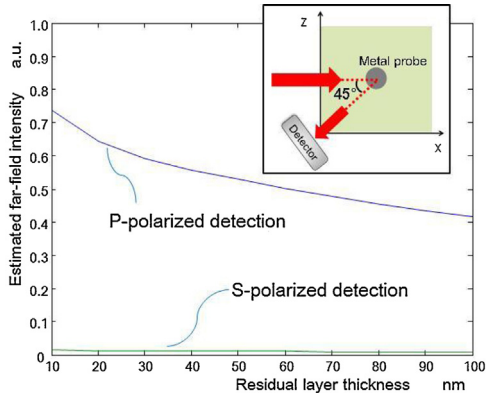

Fig. 8. Relationship between estimated far-field intensity and RLT.

shows the relationship between the degree of far-field propagating light intensity and the RLT, which was calculated based on the dipole radiation enhanced with the interaction of the metal tip and the sample surface under p-polarized incident light. Here, as shown in the upper right figure of Fig. 8, the far-field detection unit was horizontally set with the angle of 45° against the incident optics view from above, from the practical point of view that both the deterioration of the signal-to-noise ratio due to the specular reflection from the sample surface and the conflict of the incident light optics should be minimized. Even under the p-polarized incident condition, the s-polarized component of detection light can be detected, which was thought to be generated from the *Ex* component of Fig. 5 and the *Ez* component of Fig. 6. The p-polarized detection light, however, clearly depends on the RLT compared with the s-polarized component, which means good agreement with the

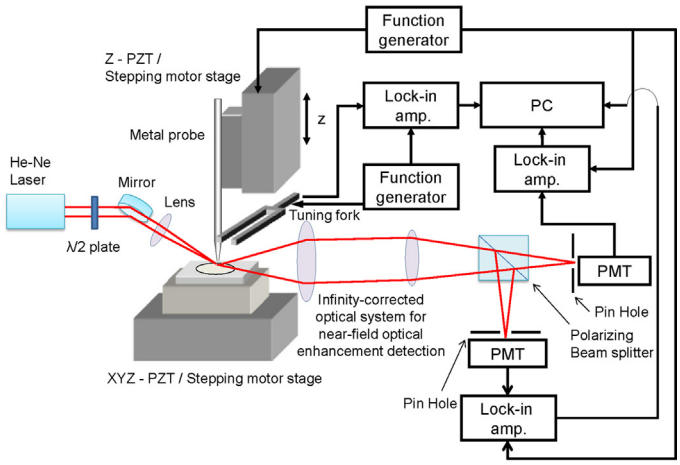

Fig. 9. Near-field optical enhancement detection system.

numerical results that the *Ey* component invades the residual layer well shown in Figs. 5 and 6.

4. Development of near-field optical enhancement detection system

A near-field optical enhancement detection system for verifying the basic concept of the proposed method was developed (Figs. 9 and 10). This system mainly consists of metal probe tip control unit, *XYZ*-PZT/stepping motor stage unit for sample positioning, and confocal microscopic unit of infinity corrected optics. A He–Ne laser with the wavelength of 632.8 nm was employed as a light source. After passing through the half wave plate for adjusting the polarization state and lens ($f = 250$), a gently focused laser beam is obliquely incident on the sample surface. Because of the 1st step for verification, commercial available metal probes with Au coat (JASCO Corp.: NPN-500) designed for near-field scanning optical microscopy (NSOM), having relatively larger size tips (tip diameter: 500 nm), are employed. A shear-force method using a tuning fork is applied for tip-sample distance control [20]. In order to get the near-field optical response with high sensitivity, a specially designed confocal microscopic unit based on infinity corrected optics with a polarizing beam splitter and two photomultiplier tubes (PMTs) is installed as shown in Fig. 9, with which we can detect both the p-polarized and the s-polarized

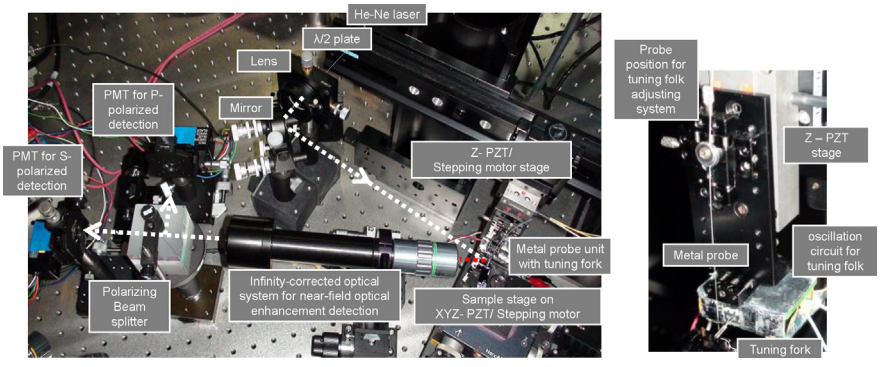

Fig. 10. Photograph of developed near-field optical enhancement detection system.

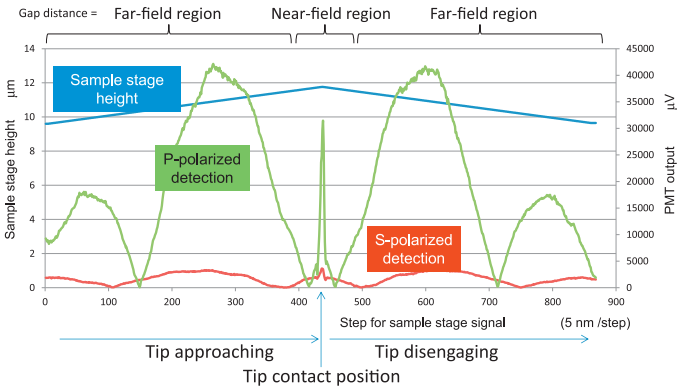

Fig. 11. Relationship between intensity of optical response and sample stage height.

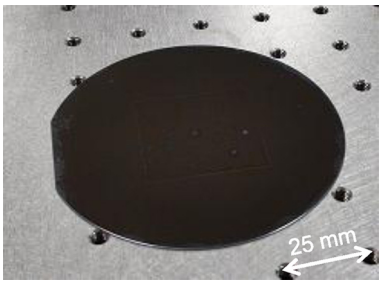

Fig. 12. Nanoimprint sample employed in the verification experiment.

signal simultaneously for studying fundamental detection characteristics.

5. Verification experiment for proposed concept

First, in order to verify the fundamental function of developed system, optical response measurement experiment from the metal tip was performed. Fig. 11 shows the relationship between the intensity of optical response from the metal tip and the sample stage height, where the gap distance between the metal tip and the sample surface was relatively controlled by changing the sample stage height. At the far-field region, periodical intensity fluctuation due to standing waves of oblique illumination and its specular reflection was observed. When the gap distance closes at about 100 nm, the detected signal sharply increases especially in the case of the p-polarized signal detection. That suggests that near-field optical enhancement interacted with the sample surface can be clearly detected with the developed system.

Finally, in order to verify the feasibility of the proposed concept, by detecting the near-field optical enhancement of metal tip with the developed system, we tried to discriminate between 10-nm-RLT and 50-nm-RLT, discrimination of which is even practically useful for adjusting the RIE conditions of the NIL processes. Fig. 12 shows the nanoimprint sample (PAK-01) employed in this experiment. Fig. 13 indicates the results with standard deviation bar of 8 experiments. We see that the near-field optical response

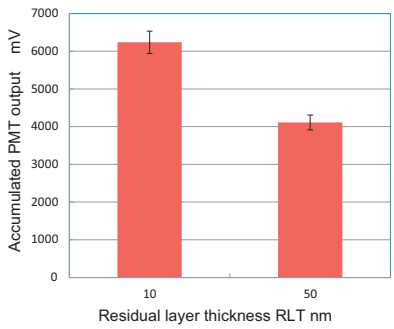

Fig. 13. Results of verification experiment.

can be detected with less than 5% deviations and the 10-nm-RLT and the 50-nm-RLT can be clearly discriminated with our developed system. A more quantitative analyses about the resolution characteristics are important future tasks.

6. Conclusions

We proposed the application of the near-field optical enhancement generated with the metal tip to the nondestructive residual layer thickness inspection. Numerical simulations based on FDTD method indicate that the perpendicular component of the enhanced near-field electric fields can be expected to include the thickness information of the residual layer with high sensitivity. Fundamental experiments using a newly developed near-field optical enhancement detection system with a specially designed confocal microscopic unit based on an infinity-corrected optical system confirmed that we can clearly discriminate between the 10- and 50-nm-RLT nondestructively.

Acknowledgments

The authors would like to profoundly thank Dr. Hideki Ina of Canon Inc., Dr. Hideyuki Wada of Molecular Imprints Inc. and Dr. Hiroshi Goto of Toshiba machine Co., Ltd. for preparing the standard residual layer thickness sample of NIL and having valuable discussions. This work was partially supported by Japan Society for the Promotion of Science (JSPS) under Grant-in-Aid for Challenging Exploratory Research Program.

References

[1] Chou SY, Krauss PR, Renstom PJ (1996) Nanoimprint Lithography. *Journal of Vacuum Science and Technology* B/14:4129–4133.
[2] Hansen HN, Hocken RJ, Tosello G (2011) Replication of Micro and Nano Surface Geometries. *Annals of CIRP* 60(2):695–714.
[3] Hocheng H, Wen TT (2010) Submicron Imprint of Trench Structures by External and Intrinsic Electromagnetic Force. *Annals of CIRP* 59(1):263–266.
[4] International Technology Roadmap for Semiconductors, 2011.
[5] Lee H (2005) Effect of Imprinting Pressure on Residual Layer Thickness in Ultraviolet Nanoimprint Lithography. *Journal of Vacuum Science and Technology* 23(3):1102–1106.
[6] Balla T, Spearing SM, Monk A (2008) An Assessment of the Process Capabilities of Nanoimprint Lithography. *Journal of Physics D Applied Physics* 41:174001–174010.
[7] Lucca DA, Brinksmeier E, Goch G (1998) Progress in Assessing Surface and Subsurface Integrity. *Annals of CIRP* 47(2):669–693.
[8] Kim TO, Kim HY, Kim CM, Ahn JH (2007) Non-Contact and In-process Measurement of Film Coating Thickness by Combining Two Principles of Eddy-Current and Capacitance Sensing. *Annals of CIRP* 56/1:509–512.
[9] Goch G, Prekel H, Patzelt S, Strobel G, Lucca DA, Stock HR, Mehner A (2004) Non-Destructive and Non-Contact Determination of Layer Thickness and Thermal Properties of PVD and Sol–Gel Layers by Photothermal Methods. *Annals of CIRP* 53/1:471–474.
[10] Semba T, Sakuma K, Tani Y, Sato H (1989) Thickness Measurement of a Metallurgically Damaged Layer on a Ground Surface Using an Acoustic Microscope. *Annals of CIRP* 38/1:549–552.
[11] Henck SA, Duncan WM, Loewenstein KM, Kuehne J (1992) In Situ Spectral Ellipsometry for Real-Time Thickness Measurement and Control. *SPIE* 1803:299–307.
[12] Trotter B, Moddel G, Ostroff R, Bogart GR (1999) Fixed-Polarizer Ellipsometry: A Simple Technique to Measure the Thickness of Very Thin Films. *Optical Engineering* 38(5):902–907.
[13] Price JR, Bingham PR, Tobin Jr KW, Karnowski TP (2003) Estimating Cross-Section Semiconductor Structure by Comparing Top-Down SEM Images. *Machine Vision Applications in Industrial Inspection XI (SPIE/IS&T)* 5011:161–170.
[14] Mayes TW, Riley MS, Edward K, Fesperman R, Suraktar A, Shahid U, Williams S (2004) Phase Imaging in the Near Field. *Annals of CIRP* 53(1):483–486.
[15] Minamiguchi S, Usuki S, Takahashi S, Takamasu K (2007) Thin Film Thickness Measurement for Evaluation of Residual Layer of Nano-Imprint Lithography using Near-Field Optics. *Proceedings of 9th ISMQC*, 167–172.
[16] Takahashi S, Minamiguchi S, Nakao T, Usuki S, Takamasu K (2009) Study on Residual Resist Layer Thickness Measurement for Nanoimprint Lithography based on Near-Field Optics. *International Journal of Surface Science and Engineering* 3(3):178–194.
[17] Kawata S, Inouye Y (1995) Scanning Probe Optical Microscopy Using a Metallic Probe Tip. *Ultramicroscopy* 57:313–317.
[18] Aigouy L, Lahrech A, GrÃsillon S, Cory H, Boccara AC, Rivoal JC (1999) Polarization Effects in Apertureless Scanning Near-Field Optical Microscopy: An Experimental Study. *Optics Letters* 24(4):187–189.
[19] Yee KS (1966) Numerical Solution of Initial Boundary Value Problems Involving Maxwell's Equations in Isotropic Media. *IEEE Trans Antennas Propagation* 14(3):302–307.
[20] Mühlschlegel P, Toquant J, Pohl DW, Hechta B (2006) Glue-Free Tuning Fork Shear-Force Microscope. *Review of Scientific Instruments* 77:016105.